Computational Thermo-Fluid Dynamics
Summer Semester 2025

Simulation of one-dimensional flow in blood vessels with a semi-implicit finite volume scheme

Carlos Gómez de Olea[1]*, Adrián Juanicotena[2]

Abstract

This report presents a numerical model for simulating one-dimensional incompressible blood flow in large arteries, a problem of physiological and engineering relevance. The flow dynamics are governed by simplified Navier–Stokes equations, specifically the conservation of mass and momentum, along with a nonlinear "tube law" relate pressure and area . The model uses a finite volume discretization on a staggered grid and treats the system in four distinct stages: convective, diffusive, pressure, and correction. The convective stage is treated explicitly and thus imposes a CFL condition, while the diffusive and pressure stages are treated implicitly to improve numerical stability. A first-order in time second-order in space integration scheme is employed, and spatial fluxes are resolved using Kolgan and Ducros-type methods. To assess accuracy and convergence, four validation test cases were performed: purely convective, purely diffusive, and two full-system tests using reference steady and unsteady solutions. The results show excellent agreement with analytical solutions, with convergence orders matching theoretical predictions in most cases.

Keywords

1D Blood Flow Model — Semi-implicit finite volume scheme — Viscoelastic vessels

[1] *MSc Aerospace Engineering student at TUM, Spanish*
[2] *MSc Computational Mechanics student at TUM, Spanish*
***e-mails**: carlos.olea@tum.de, a.juanicotena@tum.de

Contents

1. Introduction

In recent years, there has been growing interest in accurately simulating blood flow dynamics, particularly through non-invasive computational techniques [1, 2]. Patient-specific modeling of blood vessels can provide invaluable insights for diagnosis, treatment planning, and risk assessment. For example, simulations in damaged or pathological vessels may help determine whether surgical intervention is necessary or offer a better understanding of the progression of cardiovascular diseases [3, 4].

The classical approach to modeling blood flow typically involves the incompressible Navier–Stokes equations, often coupled with solid mechanics models to capture the elasticity and dynamics of vessel walls. However, full 3D fluid–structure interaction (FSI) simulations are computationally expensive, especially when applied to large vascular networks or long simulation times. [5]

To address this, reduced-order models, and in particular one-dimensional (1D) flow models, have been developed as a compromise between physiological realism and computational

efficiency [5]. These models retain the essential features of blood circulation, such as pressure and flow wave propagation, while significantly reducing computational cost. The validity and accuracy of 1D blood flow models have been demonstrated across a range of parameter regimes, including vessel elasticity, fluid viscosity, and wall mechanics (see references in [5]). These models are especially useful for simulating diverse physiological conditions, from complex arterial wave propagation to simpler venous flows.

The mathematical foundations of 1D flow modeling date back to the work of Leonhard Euler in the 18^{th} century. Modern formulations yield a system of hyperbolic partial differential equations (PDEs), governed by conservation of mass and momentum. The hyperbolic nature of the system is well-suited for numerical schemes designed to capture wave phenomena and transient dynamics.

This work focuses on a simplified 1D flow model applied to individual blood vessels, rather than the full cardiovascular system. While multi-dimensional junction models (2D/3D) are important for coupling vessels, they are beyond the scope of this study. Instead, we follow the methodology proposed in [5], and implement a semi-implicit finite volume scheme designed to balance stability and computational cost. The modeling process is structured in four distinct phases, each employing different discretization strategies. Specifically, the solution is computed sequentially by separating the system into sub-problems: a convective transport-like step, followed by a diffusive stage, a pressure stage, and a final correction stage. At each stage, the solution obtained is used as input for the next, enabling modularity and enhancing numerical stability while respecting the physical coupling between terms.

The remainder of this work is organized as follows. We begin by introducing the governing equations and modeling assumptions, followed by a detailed description of the numerical methods used, including the semi-implicit finite volume scheme and treatment of boundary conditions. We then present verification and validation results against analytical or benchmark cases, examining convergence and accuracy.

NOTE: This introduction has been written with the help of Artificial Intelligence models (Chat GPT free version) to help organize ideas. Note that this only applies to this individual section of the project.

2. Mathematical description of the model

The general methodology adopted for this work is based on the approaches described in [5, 6], although some modifications and simplifications have been introduced.

2.1 Governing Equations

The essential dynamics of hydrostatic, incompressible blood vessel flow can be described by a one-dimensional model comprising two partial differential equations representing conservation of mass and momentum:

$$\frac{\partial A}{\partial t} + \frac{\partial Au}{\partial x} = 0, \tag{1a}$$

$$\frac{\partial Au}{\partial t} + \frac{\partial \alpha Au^2}{\partial x} + \frac{A}{\rho}\frac{\partial p}{\partial x} = -su, \tag{1b}$$

where:

- $x \in [x_L, x_R] \subset \mathbb{R}$ denotes the axial coordinate.
- t represents time.
- $A(x,t)$ is the cross-sectional area of the vessel.
- $u(x,t)$ denotes the average axial flow velocity.
- $p(x,t)$ is the average pressure over the cross-section.
- ρ is the fluid density.
- The friction term is given by $s = \xi\pi\nu$, where:
  - ξ accounts for the shape of the velocity profile in a circular section.
  - ν represents the dynamic viscosity of the fluid.
- α is the momentum correction factor, which accounts for the assumed velocity profile. For simplification, it is assumed that $\alpha = 1$, corresponding to a flat velocity profile.

The system (1a)–(1b) includes three unknowns (the cross sectional area A, the mass flow $q = Au$, and the pressure p) which is why we introduce a third equation: the tube law, which links the pressure to the cross-sectional area:

$$p(x,t) = p_e + \psi(A, A_0, K) + \varphi(A, A_0)\frac{\partial A}{\partial t}, \tag{2}$$

On the one hand, the elastic pressure response ψ is described by

$$\psi(A, A_0, K) = K(x)\phi(A, A_0), \quad \text{with} \quad \phi(A, A_0) = \left(\frac{A}{A_0}\right)^m - \left(\frac{A}{A_0}\right)^n, \tag{3}$$

whereas φ is viscoelastic contribution is given by

$$\varphi(A, A_0) = \frac{\Gamma}{A_0\sqrt{A}}, \tag{4}$$

where:

- p_e is the external pressure.
- A_0 denotes the reference cross-sectional area.
- $K(x)$ is the wall stiffness coefficient, which we shall assume to be constant for the purpose of this study.
- Γ is a viscoelastic parameter.
- The exponents m and n depend on the type of vessel. This particular study will focus on arteries, for which other mathematical and physical expressions are already well known ($m = 0.5$, $n = 0$) [5].

Using the mass conservation equation (1a), and substituting into the tube law (2), the pressure gradient in (1b) becomes:

$$\frac{\partial p}{\partial x} = \frac{\partial \hat{p}}{\partial x} - \frac{\partial}{\partial x}\left(\varphi \frac{\partial (Au)}{\partial x}\right), \tag{5}$$

where $\hat{p} = p_e + \psi(A, A_0, K)$ encapsulates the purely elastic contribution to pressure variations.
Introducing the flow rate $q = Au$, and the convective flux $F(q) = q^2/A$, we can rewrite the system as:

$$\frac{\partial A}{\partial t} + \frac{\partial q}{\partial x} = 0, \tag{6a}$$

$$\frac{\partial q}{\partial t} + \frac{\partial F(q)}{\partial x} + \frac{A}{\rho}\frac{\partial p}{\partial x} - \frac{A}{\rho}\frac{\partial}{\partial x}\left(\varphi \frac{\partial q}{\partial x}\right) - \frac{A}{\rho}\frac{\partial A}{\partial t} + \frac{\partial q}{\partial x}\frac{\partial (p - \hat{p})}{\partial x} = -s\frac{q}{A}. \tag{6b}$$

where we have added and subtracted the term $\frac{A}{\rho}\frac{\partial p}{\partial x}$ to facilitate numerical implementation.

2.2 Sub-structuring of the physical problem

To solve the system numerically, we adopt a semi-implicit splitting strategy, inspired by the flux-vector splitting method described in [5]. The full system is decomposed into the following four subsystems:

- **Convective Stage.** The convective part is governed by:

$$\frac{\partial q}{\partial t} + \frac{\partial F(q)}{\partial x} = 0. \tag{7}$$

  This subsystem is solved explicitly and therefore determines the CFL time step restriction.

- **Diffusive Stage.** The diffusive subsystem, associated with vessel viscoelasticity, is solved implicitly and given by:

$$\frac{\partial q}{\partial t} - \frac{A}{\rho}\frac{\partial}{\partial x}\left(\varphi\frac{\partial q}{\partial x}\right) = 0. \tag{8}$$

- **Pressure Stage.** The pressure contribution is computed from:

$$\frac{\partial A}{\partial t} + \frac{\partial q}{\partial x} = 0, \tag{9a}$$

$$\frac{\partial q}{\partial t} + \frac{A}{\rho}\frac{\partial p}{\partial x} - \frac{A}{\rho}\frac{\partial\left(p-\hat{p}\right)}{\partial x} = -\beta s\frac{q}{A} \tag{9b}$$

  This subsystem is discretized implicitly using a staggered finite volume method.

- **Correction Stage.** The pressure computed in the previous step is used to correct the cross sectional area, and finally, the mass flow, completing our 3 unknowns. This final update accounts for all intermediate contributions and yields the velocity at the new time step.

2.3 A comment on blood vessel junctions

In this work, we restrict our analysis to the case of a single one-dimensional vessel and do not consider the additional complexities introduced by vascular junctions. However, in realistic applications, one-dimensional blood flow models are typically applied to networks of vessels that are connected at junctions, which are points where two or more vessels meet. At these junctions, special coupling conditions must be enforced to ensure the conservation of mass and momentum across the network. A common approach treats the junction as a control volume where the blood from incoming vessels is mixed and redistributed among the outgoing ones [5]. The coupling conditions are usually derived from the integral form of the Euler equations and include continuity of total pressure (accounting for momentum balance) and conservation of volumetric flow rate (mass conservation). Solving the resulting nonlinear system allows the computation of unknown variables at the junction, such as flow rates and pressures in each connected vessel [5]. Despite their importance, junctions introduce additional challenges in terms of stability and numerical implementation, which are beyond the scope of the present study.

3. Numerical Methods

3.1 Grid

To accurately resolve the spatial evolution of the conservative variables, a *staggered grid* configuration is adopted. The one-dimensional spatial domain of length L is divided into a set of non-overlapping intervals, which can be chosen to be non-uniform or not, denoted by Δx_i, following the approach described in [5, 7, 8, 9].

The grid consists of:

- **Primal cells**, indexed by i, with each cell extending from x_i to x_{i+1}. The control volumes have barycenters $x_{c,i}$.
- **Dual cells**, associated with the barycenters of the primal cells, having vertices at $x_{v,i}$ and $x_{v,i+1}$, with dual spacing $\Delta x_i^d = x_{v,i+1} - x_{v,i}$.

The discrete pressure will be computed for the primal cells, whereas the discrete axial mass flow and the averaged momentum are associated to the dual cells.

To cluster grid points near to the domain boundaries (inlet and outlet of the vessel), Chebyshev-type spacing is employed for the staggered grid points.

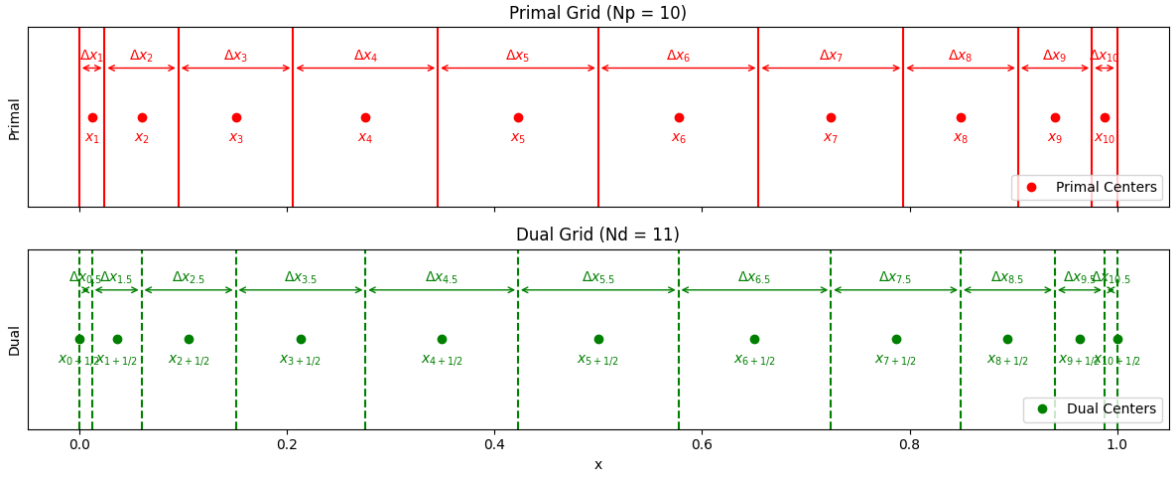

Figure 1. Example of staggered grid used for the problem (N=10)

3.2 Convective Stage

The first stage of the algorithm involves solving the convective part of the governing equation using an *explicit finite volume method*. Integrating the convective form of the conservation law over a dual control volume and applying Gauss's theorem, we obtain:

$$q^*_{i+\frac{1}{2}} = q^n_{i+\frac{1}{2}} - \frac{\Delta t}{\Delta x_i}\left(f^n_{i+1} - f^n_i\right), \tag{10}$$

The scheme is conditionally stable under a CFL constraint:

$$\Delta t \leq \text{CFL} \cdot \min_{j \in \{1,\ldots,N_d\}} \left(\frac{\Delta x_{j-\frac{1}{2}}}{2\left|u^n_{j-\frac{1}{2}}\right|} \right), \tag{11}$$

The numerical fluxes $f^n_{i+\frac{1}{2}}$ and $f^n_{i-\frac{1}{2}}$ are approximated using 2 different methods. The first is based on a first order accurate in time and space Ducros numerical scheme [10, 11]:

$$f^n_i = \frac{1}{2}\left(u^n_{i+\frac{1}{2}} + u^n_{i-\frac{1}{2}}\right)\frac{1}{2}\left(q^n_{i+\frac{1}{2}} + q^n_{i-\frac{1}{2}}\right) - \frac{1}{2}\alpha^n_i\left(q^n_{i+\frac{1}{2}} - q^n_{i-\frac{1}{2}}\right) \tag{12}$$

with:

$$\alpha^n_i = 2\ \max\left(|u^n_{i-\frac{1}{2}}|, |u^n_{i+\frac{1}{2}}|\right) \tag{13}$$

The second method consists in a higher resolution scheme based on a Kolgan-type methodology [6]. This method is aimed at improving the accuracy in space and involves replacing $q^n_{i+\frac{1}{2}}$ and $q^n_{i-\frac{1}{2}}$ by improved interpolations given by the reconstructed polynomials:

$$q^n_{i+\frac{1}{2},R}(x_i) = q^n_{i+\frac{1}{2}} + (x_i - x_{i-\frac{1}{2}})\Delta q^n_{i-\frac{1}{2}}, \quad q^n_{i+\frac{1}{2},L}(x_i) = q^n_{i+\frac{1}{2}} + (x_i - x_{i+\frac{1}{2}})\Delta q^n_{i+\frac{1}{2}},$$

where $\Delta q^n_{i+\frac{1}{2}}$ and $\Delta q^n_{i+\frac{1}{2}}$ are approximated with a minmod-type limiter as described in [5]. The discrete fluxes are then computed as:

$$f^n_i = \frac{1}{2}\left(u^n_{i+\frac{1}{2}} + u^n_{i-\frac{1}{2}}\right)\frac{1}{2}\left(q^n_{i+\frac{1}{2}} + q^n_{i-\frac{1}{2}}\right) - \frac{1}{2}\alpha^n_i\left(q^n_{i+\frac{1}{2},L} - q^n_{i-\frac{1}{2},R}\right) \tag{14}$$

with:

$$\alpha^n_i = 2\ \max\left(|u^n_{i-\frac{1}{2},L}|, |u^n_{i+\frac{1}{2},R}|\right) \tag{15}$$

In later sections, the convergence of both methods will be explored.

3.3 Diffusive Stage

The second stage addresses the diffusive transport, solved via an *implicit finite volume method* using the Backward Time Centered Space (BTCS) scheme. After obtaining the intermediate state q^* from the convective update, the diffusive part is solved as follows:

$$q^{**}_{i+\frac{1}{2}} = q^{*}_{i+\frac{1}{2}} + \frac{\Delta t}{\Delta x_{i+\frac{1}{2}}} \frac{A^n_{i+\frac{1}{2}}}{\rho} \left[\varphi^n_+ \frac{q^{**}_{i+\frac{3}{2}} - q^{**}_{i+\frac{1}{2}}}{\Delta x_{i+1}} + \varphi^n_- \frac{q^{**}_{i+\frac{1}{2}} - q^{**}_{i-\frac{1}{2}}}{\Delta x_i} \right] \tag{16}$$

where:

$$A^n_{i+\frac{1}{2}} = \frac{A(p^n_i) + A(p^n_{i+1})}{2} \tag{17}$$

After re-arranging mathematically, equation 16 can be written into a tridiagonal system of equations, which can be expressed in matrix form as:

$$\mathbf{D}\mathbf{q}^{**} = \mathbf{v}, \tag{18}$$

where (and note that this was corrected from the mistake in [5]):

$$\mathbf{v} = \frac{\Delta x_{i+\frac{1}{2}}}{A^n_{i+\frac{1}{2}}} q^*_{i+\frac{1}{2}} \tag{19}$$

and $\mathbf{D}$ is a tridiagonal matrix with entries:

$$a_i = -\frac{\Delta t}{\rho} \frac{\varphi^n_-}{\Delta x_i}, \quad b_i = \frac{\Delta x_{i+\frac{1}{2}}}{A^n_{i+\frac{1}{2}}} + \frac{\Delta t}{\rho} \frac{\varphi^n_-}{\Delta x_i} + \frac{\Delta t}{\rho} \frac{\varphi^n_+}{\Delta x_{i+1}}, \quad c_i = -\frac{\Delta t}{\rho} \frac{\varphi^n_+}{\Delta x_{i+1}},$$

Since $\mathbf{D}$ is symmetric positive definite and posses interesting sparse characteristics, the system can be easily and efficiently solved using simple python commands, obtaining the intermediate solution for the diffusive stage q^{**}. Note that the scheme is unconditionally stable, first order accurate in time, and second order accurate in space.

3.4 Pressure and Correction Stage

The last part of the process consists in solving the pressure subsystem, which was described in equation 9b. The implicit discretization of the continuity equation yields:

$$M(p_i^{n+1}) = M(p_i^n) - \Delta t \left(q_{i+\frac{1}{2}}^{n+1} - q_{i-\frac{1}{2}}^{n+1} \right), \tag{20}$$

where $M(p_i) = A(x_i)\Delta x_i$ is the fluid mass contained in the i-th cell. At the same time, as we will consider that the viscosity is null for the sake of this project, the momentum equation can be written as:

$$q_{i+\frac{1}{2}}^{n+1} = q_{i+\frac{1}{2}}^{**} - \frac{\Delta t}{\Delta x_{i+\frac{1}{2}}} \frac{A_{i+\frac{1}{2}}^n}{\rho} (p_{i+1}^{n+1} - p_i^{n+1}) + \frac{\Delta t}{\Delta x_{i+\frac{1}{2}}} \frac{A_{i+\frac{1}{2}}^n}{\rho} \left((p - \hat{p})_{i+1}^n - (p - \hat{p})_i^n \right) \tag{21}$$

Merging these last 2 equations and after some mathematical development and rearrangement, we get:

$$\begin{aligned} M(p_i^{n+1}) - \frac{\Delta t^2}{\Delta x_{i-\frac{1}{2}}} \frac{A_{i-\frac{1}{2}}^n}{\rho} p_{i-1}^{n+1} + \Delta t^2 \left[\frac{1}{\Delta x_{i+\frac{1}{2}}} \frac{A_{i+\frac{1}{2}}^n}{\rho} + \frac{1}{\Delta x_{i-\frac{1}{2}}} \frac{A_{i-\frac{1}{2}}^n}{\rho} \right] p_i^{n+1} \\ - \frac{\Delta t^2}{\Delta x_{i+\frac{1}{2}}} \frac{A_{i+\frac{1}{2}}^n}{\rho} p_{i+1}^{n+1} = M(p_i^n) - \Delta t \left(q_{i+\frac{1}{2}}^{**} - q_{i-\frac{1}{2}}^{**} \right) \\ - \Delta t^2 \left[\frac{A_{i+\frac{1}{2}}^n}{\rho \Delta x_{i+\frac{1}{2}}} \left((p - \hat{p})_{i+1}^n - (p - \hat{p})_i^n \right) - \frac{A_{i-\frac{1}{2}}^n}{\rho \Delta x_{i-\frac{1}{2}}} \left((p - \hat{p})_i^n - (p - \hat{p})_{i-1}^n \right) \right]. \end{aligned} \tag{22}$$

This can be written in a more compact form as the following problem:

$$M(p^{n+1}) + T p^{n+1} = b^n, \tag{23}$$

where

- $M = \text{diag}(M(p_i^{n+1}))$ is a vector function;
- T is a symmetric positive-definite matrix, whose entries are

$$a_i = -\frac{\Delta t^2}{\Delta x_{i-\frac{1}{2}}} \frac{A_{i-\frac{1}{2}}^n}{\rho}, \quad b_i = \frac{\Delta t^2}{\Delta x_{i-\frac{1}{2}}} \frac{A_{i-\frac{1}{2}}^n}{\rho} + \frac{\Delta t^2}{\Delta x_{i+\frac{1}{2}}} \frac{A_{i+\frac{1}{2}}^n}{\rho}, \quad c_i = -\frac{\Delta t^2}{\Delta x_{i+\frac{1}{2}}} \frac{A_{i+\frac{1}{2}}^n}{\rho},$$

3.4.1 Elastic arteries case

We know that for the case of elastic arteries ($m = 0.5,\ n = 0$), and considering a null viscoelastic parameter Γ, the tube law can be inverted to express the area in the time step $n+1$ in terms of the pressure in step $n+1$:

$$A_i^{n+1} = A_0 \left(1 + \frac{p_i^{n+1} - p_e}{K} \right)^2 \tag{24}$$

which means that the term $M(p^{n+1}) = A^{n+1}\Delta x_i$ will induce non-linear terms for p^{n+1}. Consequently, system 23 is solved thanks to a Newton algorithm to obtain p^{n+1}.

Once the new pressure is computed, we may now estimate the area in the temporal step $n+1$ by the equation 3.4.1. Finally, we may compute the mass flow at step $n+1$, q^{n+1} via equation 21

3.4.2 General Tube case

The value of $\mathbf{M}(\mathbf{p})$ is highly non-linear for viscous tubes or tubes where the parameters of $m \& n$ are different from those of the artery. In such cases, equation 20 cannot be solved with a standard Newton solver [12]. For this reason a "nested Newton" approach [13, 14] is introduced.

The key idea is to decompose the nonlinearity by splitting the derivative of each component $M_i(p)$ into the difference of two non-negative, non-decreasing functions:

$$\frac{dM_i(p)}{dp} = s_i(p) - r_i(p), \quad \text{with} \quad 0 \le r_i(p) \le s_i(p). \tag{25}$$

This is done using a Jordan decomposition as described in [13, 14] . Functions $s_i(p)$ and $r_i(p)$ are defined as:

$$s_i(p) = \begin{cases} c_i(p), & p \le p_v, \\ c_i(p_v), & p > p_v, \end{cases} \quad r_i(p) = \begin{cases} 0, & p \le p_v, \\ s_i(p) - c_i(p), & p > p_v, \end{cases} \tag{26}$$

where $c_i(p) = \frac{dM_i(p)}{dp}$ and p_v marks the point where $c_i(p)$ changes from increasing to decreasing.

Using this knowledge, the nonlinear term is written as a difference of two monotonic functions:

$$\boldsymbol{M}(\boldsymbol{p}^{n+1}) = \boldsymbol{M}_1(\boldsymbol{p}^{n+1}) - \boldsymbol{M}_2(\boldsymbol{p}^{n+1}). \tag{27}$$

Here, $\boldsymbol{M}_1$ is piecewise linear for $p > p_v$:

$$M_1(p) = \begin{cases} M(p), & p \le p_v, \\ M(p_v) + M'(p_v)(p - p_v), & p > p_v, \end{cases} \quad \text{with} \quad M_2(p) = M_1(p) - M(p). \tag{28}$$

with:

$$p_v = p_e + K\left(\left(\frac{n(n-1)}{m(m-1)}\right)^{\frac{m}{m-n}} - \left(\frac{n(n-1)}{m(m-1)}\right)^{\frac{n}{m-n}}\right) \tag{29}$$

In the nested Newton approach, the outer iteration linearizes $\boldsymbol{M}_2$, while the inner iteration linearizes both $\boldsymbol{M}_1$ and $\boldsymbol{M}_2$, enabling efficient and robust convergence. To do this we introduce the following matrices:

$$R(\boldsymbol{p}) = diagonal(\frac{\partial \boldsymbol{M_1}(\boldsymbol{p})}{\partial \boldsymbol{p}}),\ Q(\boldsymbol{p}) = diagonal(\frac{\partial \boldsymbol{M_2}(\boldsymbol{p})}{\partial \boldsymbol{p}}) \tag{30}$$

The complete nested Netwon algorithm is described in 1. To get the values for $\boldsymbol{M}_1(\boldsymbol{p})$, $\boldsymbol{M}_2(\boldsymbol{p})$ we need to remember that $M(p_i^*) = A(p_i^*)\Delta x_i$. To obtain the value of $A(p_i^*)$ one needs to solve the the tube law (see equation 2) for A^*. The time derivative is approximated by backward time derivative, leaving us the following equation with a "normal" newton algorithm:

$$p_e + K \cdot \left(\left(\frac{A^*}{A_0}\right)^m - \left(\frac{A^*}{A_0}\right)^n\right) + \frac{\Gamma}{A_o\sqrt{A^*}}\frac{A^* - A^n}{\Delta t} - p^* = 0 \tag{31}$$

In addition, the term $\partial M_j(p_i^*)/\partial p_i^*$ is solved through a finite difference scheme centered on i:

$$\frac{\partial M_j(p_i^*)}{\partial p_i^*} = \frac{M_j(p_i^* + \epsilon) - M_j(p_i^* - \epsilon)}{2\epsilon}, \text{ with } j \in [1,2] \text{ and } \epsilon \in [1e^{-4}, 1e^{-8}] \cdot min(|p_i^*|, 1) \tag{32}$$

Note that the lower bounds of ϵ were chosen to avoid surpassing the machine precision as well as relative errors.

Algorithm 1 Nested Newton Method for Solving $\boldsymbol{M}_1(\boldsymbol{p}) - \boldsymbol{M}_2(\boldsymbol{p}) + \boldsymbol{T}\boldsymbol{p} = \boldsymbol{b}$

Set $\boldsymbol{p}^0 <= p_v$
for $n = 1$ to N **do** ▷ Inner loop (linearizing $\boldsymbol{M}_2$)
  Compute $\boldsymbol{M}_1(\boldsymbol{p}^n)$, $\boldsymbol{M}_2(\boldsymbol{p}^n)$, $\frac{\partial \boldsymbol{M}_1(\boldsymbol{p}^n)}{\partial \boldsymbol{p}}$, $\frac{\partial \boldsymbol{M}_2(\boldsymbol{p}^n)}{\partial \boldsymbol{p}}$
  $\boldsymbol{R} \leftarrow \mathrm{diag}\left(\frac{\partial \boldsymbol{M}_1}{\partial \boldsymbol{p}}\right)$, $\boldsymbol{Q} \leftarrow \mathrm{diag}\left(\frac{\partial \boldsymbol{M}_2}{\partial \boldsymbol{p}}\right)$
  $\boldsymbol{J} \leftarrow \boldsymbol{R} + \boldsymbol{T} - \boldsymbol{Q}$
  $\boldsymbol{r}_n \leftarrow \boldsymbol{M}_1 - \boldsymbol{M}_2 + \boldsymbol{T}\boldsymbol{p}^n - \boldsymbol{b}$
  if $\|\boldsymbol{r}^n\| \leq \varepsilon$ **then**
    Converged → exit outer loop
    break
  end if
  $\boldsymbol{d}^n \leftarrow \boldsymbol{b} + \boldsymbol{M}_2 - \boldsymbol{Q}\boldsymbol{p}^n$
  for $m = 1$ to N **do** ▷ Inner loop (linearizing $\boldsymbol{M}_1$)
    $\boldsymbol{r}^{nm} \leftarrow \boldsymbol{M}_1 + (\boldsymbol{T} - \boldsymbol{Q})\boldsymbol{p}^{n,.m} - \boldsymbol{d}$
    if $\|\boldsymbol{r}^{nm}\| \leq \varepsilon$ **then**
      $\boldsymbol{p}^n \leftarrow \boldsymbol{p}^{n,m}$
      break
    end if
    $\boldsymbol{f}^{n,m} \leftarrow \boldsymbol{R}\boldsymbol{p} - \boldsymbol{M}_1 + \boldsymbol{d}^n$
    Solve $\boldsymbol{J}\boldsymbol{p}_{\mathrm{new}} = \boldsymbol{f}^{n,m}$
    $\boldsymbol{p} \leftarrow \boldsymbol{p}_{\mathrm{new}}$
    Update $\boldsymbol{M}_1(\boldsymbol{p}^{n,m})$
    Update $\boldsymbol{R} \leftarrow \mathrm{diag}\left(\frac{d\boldsymbol{M}_1}{d\boldsymbol{p}}\right)$
    Update $\boldsymbol{J} \leftarrow \boldsymbol{R} + \boldsymbol{T} - \boldsymbol{Q}$
  end for
end for

3.5 The θ method

To enhance the temporal accuracy of the semi-implicit splitting approach, a θ-method is incorporated into the numerical scheme. This method introduces a time-weighted average for the primary variables, momentum flux q and pressure p, evaluated at an intermediate time level $t^{n+\theta}$:

$$q^{n+\theta} = \theta q^{n+1} + (1-\theta) q^n, \tag{33}$$
$$p^{n+\theta} = \theta p^{n+1} + (1-\theta) p^n, \tag{34}$$

where θ is a parameter in the range $\left(\frac{1}{2}, 1\right]$.
Substituting these expressions into the time-discrete equations leads to modified forms of the diffusive, continuity, and momentum equations:

Updated diffusive equation:

$$q^{**} = q^* + (1-\theta)\Delta t \frac{1}{\rho A(p^n)} \frac{\partial}{\partial x}\left(\phi^n \frac{\partial q^n}{\partial x}\right) + \theta \Delta t \frac{1}{\rho A(p^n)} \frac{\partial}{\partial x}\left(\phi^n \frac{\partial q^{**}}{\partial x}\right) \tag{35}$$

Updated continuity equation:

$$A(p^{n+1}) = A(p^n) - (1-\theta)\Delta t \frac{\partial q^n}{\partial x} - \theta \Delta t \frac{\partial q^{n+1}}{\partial x} \tag{36}$$

Updated momentum equation:

Choosing $\theta = 1$ recovers the original first-order accurate scheme in time. Setting $\theta = \frac{1}{2}$ results in the classical Crank–Nicolson method, which provides second-order accuracy in time. However, it is well known that Crank-Nicolson produces spurious oscillations in the presence of discontinuities, therefore in case of fluid with discontinuities $\theta > \frac{1}{2}$. As most blood flows are continuous and smooth [5], the choice $\theta = \frac{1}{2}$ remains a good choice for better temporal accuracy.

3.5.1 Diffusive stage discretization

To discretize the diffusive equation under the θ method, we need to modify equation 18:

$$\mathbf{v} = \frac{\Delta x_{i+\frac{1}{2}}}{A^n_{i+\frac{1}{2}}} q^*_{i+\frac{1}{2}} + (1-\theta) \cdot \left(\frac{\Delta t}{\rho}\frac{\varphi^n_-}{\Delta x_i} q^n_{i-\frac{1}{2}} - \left(\frac{\Delta t}{\rho}\frac{\varphi^n_-}{\Delta x_i} + \frac{\Delta t}{\rho}\frac{\varphi^n_+}{\Delta x_{i+1}}\right) q^n_{i+\frac{1}{2}} + \frac{\Delta t}{\rho}\frac{\varphi^n_+}{\Delta x_{i+1}} q^n_{i+\frac{3}{2}}\right) \tag{38}$$

where $\mathbf{D}$ is a tridiagonal matrix with entries:

$$a_i = -\theta\frac{\Delta t}{\rho}\frac{\varphi_-^n}{\Delta x_i}, \quad b_i = \frac{\Delta x_{i+\frac{1}{2}}}{A^n_{i+\frac{1}{2}}} + \theta\left(\frac{\Delta t}{\rho}\frac{\varphi_-^n}{\Delta x_i} + \frac{\Delta t}{\rho}\frac{\varphi_+^n}{\Delta x_{i+1}}\right), \quad c_i = -\theta\frac{\Delta t}{\rho}\frac{\varphi_+^n}{\Delta x_{i+1}},$$

3.5.2 Pressure stage discretization

We now focus our attention into equation 21

$$q^{n+1}_{i+\frac{1}{2}} = q^{**}_{i+\frac{1}{2}} - \theta\frac{\Delta t}{\Delta x_{i+\frac{1}{2}}}\frac{A^n_{i+\frac{1}{2}}}{\rho}(p^{n+1}_{i+1} - p^{n+1}_i) - (1-\theta)\frac{\Delta t}{\Delta x_{i+\frac{1}{2}}}\frac{A^n_{i+\frac{1}{2}}}{\rho}(p^n_{i+1} - p^n_i) + \frac{\Delta t}{\Delta x_{i+\frac{1}{2}}}\frac{A^n_{i+\frac{1}{2}}}{\rho}\left((p-\hat{p})^n_{i+1} - (p-\hat{p})^n_i\right) \tag{39}$$

Merging these in the continuity equation, the new pressure subsystem to solve becomes:

$$\begin{aligned}
&M(p^{n+1}_i) - \frac{(\theta\Delta t)^2}{\Delta x_{i-\frac{1}{2}}}\frac{A^n_{i-\frac{1}{2}}}{\rho}p^{n+1}_{i-1} + (\theta\Delta t)^2\left[\frac{1}{\Delta x_{i+\frac{1}{2}}}\frac{A^n_{i+\frac{1}{2}}}{\rho} + \frac{1}{\Delta x_{i-\frac{1}{2}}}\frac{A^n_{i-\frac{1}{2}}}{\rho}\right]p^{n+1}_i \\
&\quad - \frac{(\theta\Delta t)^2}{\Delta x_{i+\frac{1}{2}}}\frac{A^n_{i+\frac{1}{2}}}{\rho}p^{n+1}_{i+1} = M(p^n_i) - \theta\Delta t\left(q^{**}_{i+\frac{1}{2}} - q^{**}_{i-\frac{1}{2}}\right) \\
&\quad - (\theta\Delta t)^2\left[\frac{A^n_{i+\frac{1}{2}}}{\rho\Delta x_{i+\frac{1}{2}}}\left((p-\hat{p})^n_{i+1} - (p-\hat{p})^n_i\right) - \frac{A^n_{i-\frac{1}{2}}}{\rho\Delta x_{i-\frac{1}{2}}}\left((p-\hat{p})^n_i - (p-\hat{p})^n_{i-1}\right)\right] \\
&\quad + (1-\theta)\frac{\theta\Delta t^2}{\Delta x_{i-\frac{1}{2}}}\frac{A^n_{i-\frac{1}{2}}}{\rho}p^n_{i-1} - (1-\theta)\theta\Delta t^2\left[\frac{1}{\Delta x_{i+\frac{1}{2}}}\frac{A^n_{i+\frac{1}{2}}}{\rho} + \frac{1}{\Delta x_{i-\frac{1}{2}}}\frac{A^n_{i-\frac{1}{2}}}{\rho}\right]p^n_i \\
&\quad + (1-\theta)\frac{\theta\Delta t^2}{\Delta x_{i+\frac{1}{2}}}\frac{A^n_{i+\frac{1}{2}}}{\rho}p^n_{i+1}
\end{aligned} \tag{40}$$

4. Validation and Results

To verify the precision and robustness of the numerical implementation, a series of validation tests were conducted under controlled conditions. These include a *simplified convective problem*, a *simplified diffusive problem*, a *complete steady problem*, and a *complete unsteady problem*. All test cases share the following common settings: periodic boundary conditions, null viscosity, fluid density $\rho = 1050\,\mathrm{kg/m^3}$, external pressure $p_e = 0$, wall model parameters $m = 0.5$ and $n = 0$ (corresponding to an elastic artery). For the relevant tests, the wall stiffness coefficient K is assumed to be constant and equal to a reference value K_{ref}.

The convective and diffusive problems are designed to isolate the influence of pure advection and diffusion, respectively. In contrast, the complete steady and unsteady problems incorporate both effects, along with wall elasticity. The key parameters specific to each test case are summarized in Table 1.

Test Case	A_0 [m^2]	K	Γ	t_F [s]	θ
Simplified convective	1	–	–	0.1	–
Simplified diffusive	1	–	1	0.1	–
Complete steady	3.1416×10^{-4}	80	0	0.1	0.5
Complete unsteady	3.1416×10^{-4}	80	1	0.1	0.5

Table 1. Simulation parameters used in the validation test cases. All simulations assume $L = 1$ m, $\mu = 0$, $\rho = 1050\,\mathrm{kg/m^3}$, $p_e = 0$, $m = 0.5$, $n = 0$, and periodic boundary conditions.

Test Case	Np	Δt [s]
Simplified convective	[10, 50, 100, 200, 500, 1000, 5000]	$1 \cdot 10^{-5}$
Simplified diffusive	[10, 15, 25, 40, 50, 75, 100, 150, 200]	$1 \cdot 10^{-4}$
Complete steady	[10, 20, 40, 80]	$[50, 25, 12.5, 6.25] \cdot 10^{-4}$
Complete unsteady	[10, 20, 40, 80, 160]	$[50, 25, 12.5, 6.25, 3.125] \cdot 10^{-4}$

Table 2. Discretization Parameters used in the validation test cases.

4.1 Test 1: Simplified convective problem

To test the convective stage explained in 3.2, let's first consider a purely convective problem, modelled mathematically by equation 10. For the sake of simplicity, we shall assume that the area is constant over time and across the full vessel:

$$A(x,t)_{convective} = A_0 \tag{41}$$

As the pressure is also directly dependent on the cross sectional area of the vessel, the momentum balance equation described in 7 can be simplified to:

$$\frac{\partial q}{\partial t} + \frac{1}{A_0}\frac{\partial q^2}{\partial x} = 0 \tag{42}$$

After applying the chain law to the derivative in x, this becomes:

$$\frac{\partial q}{\partial t} + \frac{2q}{A_0}\frac{\partial q}{\partial x} = 0 \tag{43}$$

This is a first-order quasilinear partial differential equation and can be solved using the method of characteristics. The idea is to reduce the PDE to an ODE along characteristic curves $x(t)$ defined by:

$$\frac{dx}{dt} = \frac{2q}{A_0}, \qquad \frac{dq}{dt} = 0 \tag{44}$$

This means that the solution q is constant along each characteristic, and the characteristics themselves are governed by the value of q. Therefore, characteristics originating from different points may move at different speeds, potentially leading to shock formation.
Assume the initial condition is a sinusoidal wave:

$$q(x,0) = \sin\left(\frac{2\pi x}{L}\right) \tag{45}$$

Label the initial position of a characteristic as x_0. Then along the characteristic that starts at x_0, the value of q remains:

$$q = \sin\left(\frac{2\pi x_0}{L}\right) \tag{46}$$

The characteristic curve from x_0 follows:

$$x(t) = x_0 + \frac{2t}{A_0}\sin\left(\frac{2\pi x_0}{L}\right) \tag{47}$$

Inverting this relationship allows us to find $x_0 = x_0(x,t)$, and therefore, the solution at time t and position x is:

$$q(x,t) = \sin\left(\frac{2\pi x_0(x,t)}{L}\right) \tag{48}$$

This expression defines the analytical solution implicitly: note that one must solve iteratively for x_0 with a Newton algorithm for every instant of time. It remains valid as long as the mapping from x_0 to x is invertible, i.e., before characteristics cross. At that time instant, a shock may form when the Jacobian $\partial x/\partial x_0$ vanishes. We compute:

$$\frac{\partial x}{\partial x_0} = 1 + \frac{4\pi t}{A_0 L}\cos\left(\frac{2\pi x_0}{L}\right) \tag{49}$$

Mathematically, it can be derived that the first time a shock forms is when this derivative becomes zero for the first time, that is at:

$$t_s = \frac{A_0 L}{4\pi} \tag{50}$$

Therefore, the analytical solution described above is valid only for $t < t_s$. After this time, characteristics may intersect, and the solution becomes multi-valued. To handle this, one should introduce shock-capturing numerical methods.

The numerical solution for the mass flow is presented in figure 2. Both the Ducros and Kolgan methods described in 3.2 have been simulated and compared to the analytical solution described in the previous paragraphs. Although the shape of the analytical solution is in general well captured, the numerical scheme seems to struggle close to extremes.

Additionally, a convergence study has been performed using both methods (see Figure 3). According to [5], we should expect the Ducros scheme to offer first order accuracy in space and time, and the Kolgan method to slighlty improve the convergence in space (how much improvement though is unknown). Although for smaller grids ($N_p \approx 5$), the Kolgan scheme appears to offer slightly higher accuracy, both methods exhibit very similar convergence behaviour overall. A linear fit of the L2 error vs the number of grid points was performed. The observed convergence rate is not quite of first order as expected, but slightly lower

(0.71 in both cases). The reason for this is unknwown, although the numerical parameters set for the recursive obtention of the analytical solution via a Newton method (particularly the tolerance), could be involved.

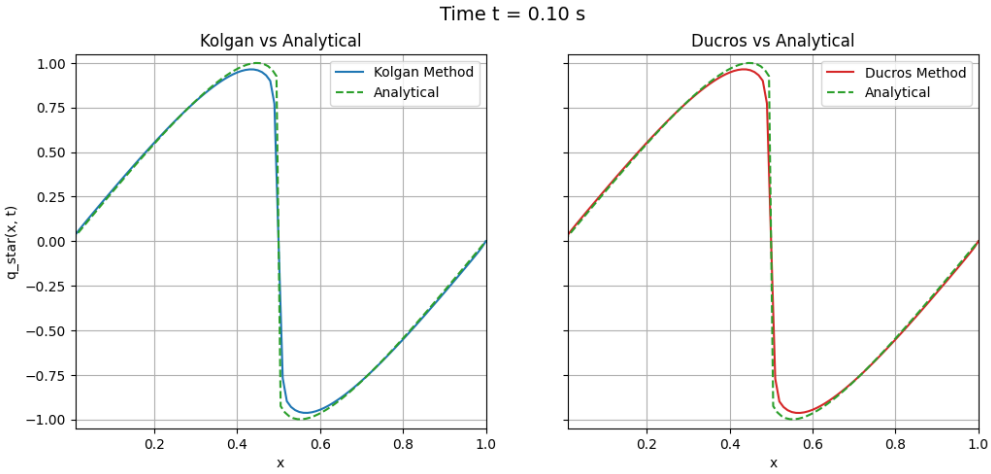

Figure 2. Mass flow solution at $t = t_F$ for purely convective simplified problem ($N_p = 1000$, $L = 1\ m$, $A = A_0 = 1\ m^2$, $\Delta t = 10^{-5}\ s$)

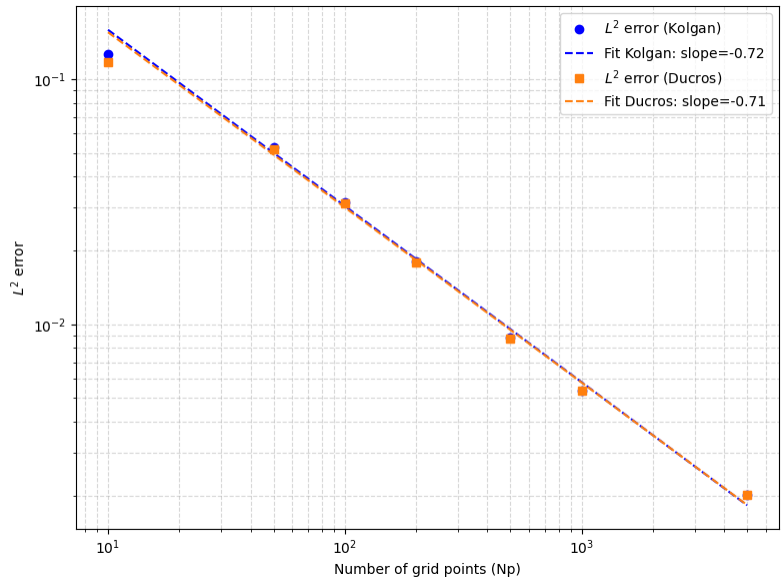

Figure 3. Convergence of numerical solution for purely convective problem

4.2 Test 2: Simplified diffusive problem

Let us now isolate the diffusion stage, modeled by equation 8. Assuming again that the area is constant in time and space and equal to A_0, the equation simplifies to:

$$\frac{\partial q}{\partial t} - \frac{A_0}{\rho}\varphi(A_0)\frac{\partial^2 q}{\partial x} = 0 \tag{51}$$

Equation 4.2 is in fact a linear diffusion equation in one spatial dimension. In our case, we consider a finite domain $x \in [0, L]$ with periodic boundary conditions $q(0,t) = q(L,t) = 0$, and an initial condition of the form $q(x,0) = \sin\left(\frac{n\pi x}{L}\right)$, which corresponds to a single mode in a Fourier sine series expansion. The solution to the diffusion equation in this setting is given by:

$$q(x,t) = \sum_{n=1}^{\infty} B_n \sin\left(\frac{n\pi x}{L}\right) \exp\left(-\Phi\left(\frac{n\pi}{L}\right)^2 t\right), \tag{52}$$

where B_n are the Fourier coefficients of the initial condition. If the initial condition consists of a pure second mode, i.e., $q(x,0) = \sin\left(\frac{2\pi x}{L}\right)$, then all coefficients $B_n = 0$ for $n \neq 2$, and the solution simplifies to:

$$q(x,t) = \sin\left(\frac{2\pi x}{L}\right) \exp\left(-\Phi\left(\frac{2\pi}{L}\right)^2 t\right). \tag{53}$$

This form shows the exponential decay of the second harmonic over time due to diffusive effects, with the decay rate increasing with the square of the mode number.

As the diffusive stage involves solving a matricial system of equations, its computational cost is notably higher than that of the convective system, and thus smaller meshes have been tried out. Just like in the previous section, the numerical solution for the mass flow is presented in figure 4 in comparison to the analytical solution described in the previous paragraphs.

Additionally, the L^2 error of the numerical solution for various grid sizes was represented in figure 5. Remember that we should be expecting the numerical scheme to be second order accurate in space, and first order accurate in time. A linear fit was performed to determine the observed convergence rate, yielding a value of 2.12 for grid sizes between 10 and 100 points, closely aligning with expectations. However, for larger meshes (150 or 200 points for instance), convergence becomes apparently faster for reasons yet unknown. These last points were not taken into account for the linear fit.

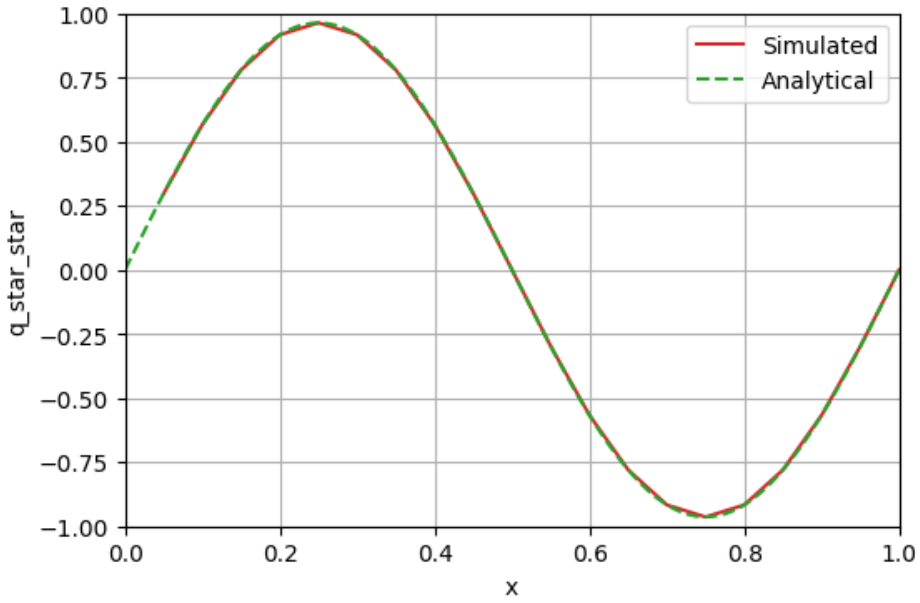

Figure 4. Mass flow solution at $t = t_F$ for purely diffusive simplified problem ($N_p = 50$, $L = 1\ m$, $A = A_0 = 1\ m^2$, $\Delta t = 10^{-4}\ s$)

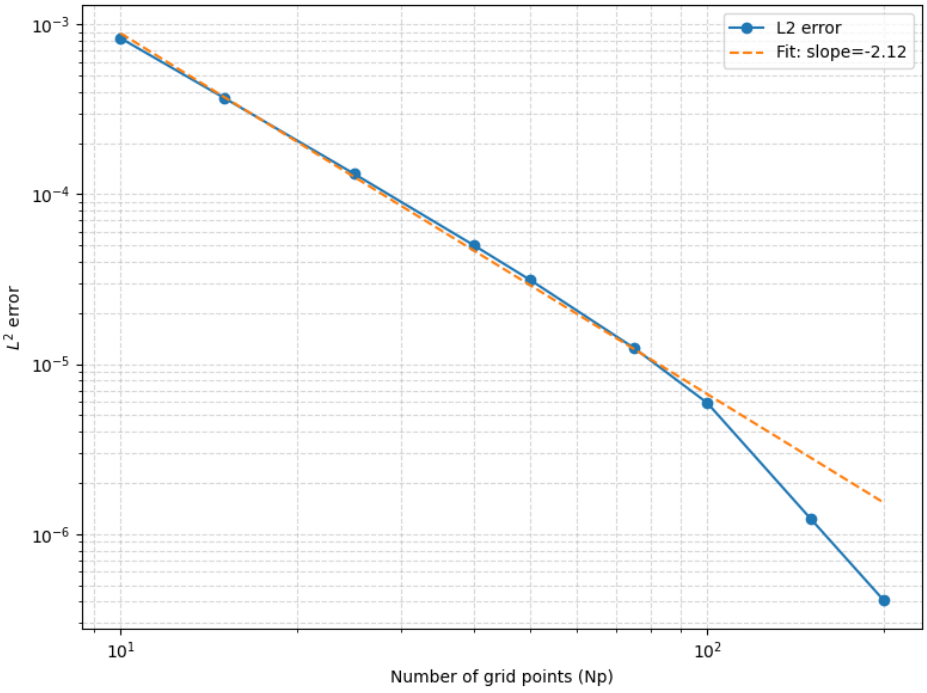

Figure 5. Convergence of numerical solution for purely diffusive problem

4.3 Test 3: Complete steady problem

As suggested in [5], an additional test was performed with the "reference" exact solution given by

$$\begin{aligned} A(x,t) &= (\sin(2\pi x)+4)^{-1} \\ q(x,t) &= 1 \end{aligned} \tag{54}$$

With equation 2, and introducing the corresponding K, m and n parameters in 3 and 4, we also know the explicit expression of the pressure:

$$p(x,t) = p_e + K_{ref}\left(\sqrt{\frac{A(x,t)}{A_0}} - 1\right) \tag{55}$$

For this solution test to be valid, we need to modify the equations for the different stages by numerically adding new "forcing" source terms containing the non-zero terms that arise when replacing 54 in equations 7, 8 and 9b such that the equations become:

- **Convective Stage:** $\dfrac{\partial q}{\partial t} + \dfrac{\partial F(q)}{\partial x} = \hat{s}_{\text{convective}}$
- **Diffusive Stage:** $\dfrac{\partial q}{\partial t} - \dfrac{A}{\rho}\dfrac{\partial}{\partial x}\left(\varphi\dfrac{\partial q}{\partial x}\right) = \hat{s}_{\text{diffusive}}$
- **Pressure Stage:** $\dfrac{\partial q}{\partial t} + \dfrac{A}{\rho}\dfrac{\partial p}{\partial x} - \dfrac{A}{\rho}\dfrac{\partial\left(p-\hat{p}\right)}{\partial x} = -\beta s\dfrac{q}{A} + \hat{s}_{\text{pressure}}$

Given that we are dealing with a problem with null viscosity ($s = 0$) and introducing relations 54 and 55 in the previous equations, $\hat{s}$ can be mathematically derived for all three stages:

$$\hat{s}_{\text{convective}} = 2\pi\cos(2\pi x) \tag{56}$$

$$\hat{s}_{\text{diffusive}} = 0 \tag{57}$$

$$\hat{s}_{\text{pressure}} = -\frac{\pi K\cos(2\pi x)}{\rho\sqrt{A_0}}A(x,t)^{\frac{5}{2}} \tag{58}$$

Each numerical correction is applied individually at all time steps of every stage. The numerical solution at $t = t_F$ is shown in figure 6 and plotted against the analytical reference solution (dashed line). For the steady test, it appears as though the numerical scheme is accurately prediciting the shape of the "reference" analytical solutions, pointing to a correct integration of the forced source terms and the general numerical scheme. However, some deviation to the analytical solution may be observed. This is especially visible for the mass flow, which presents spatial fluctuations with respect to its expected costant value. In terms

of the pressure and the cross sectional area, the numerical solution seems to have been slightly displaced in space.

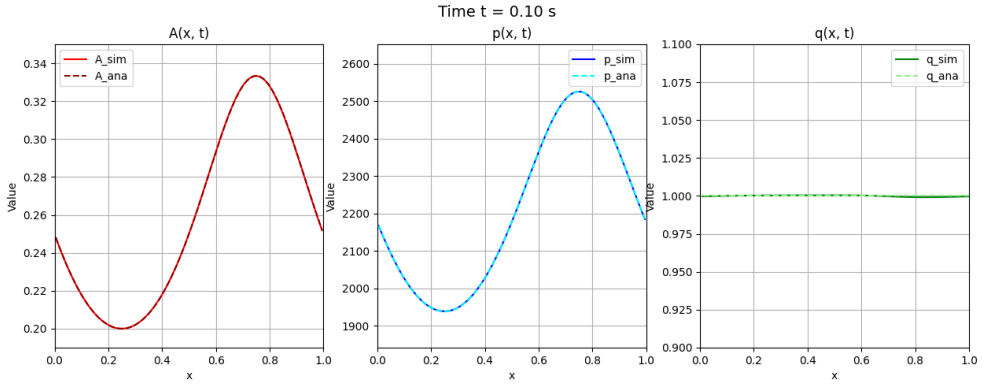

Figure 6. Cross sectional area, mass flow and pressure solution at $t = t_F$ for steady test ($N_p = 30$, $L = 1$ m, $A = A_0 = 3.1416\text{e-}4\ m^2$, $\Delta t = 10^{-3}$ s)

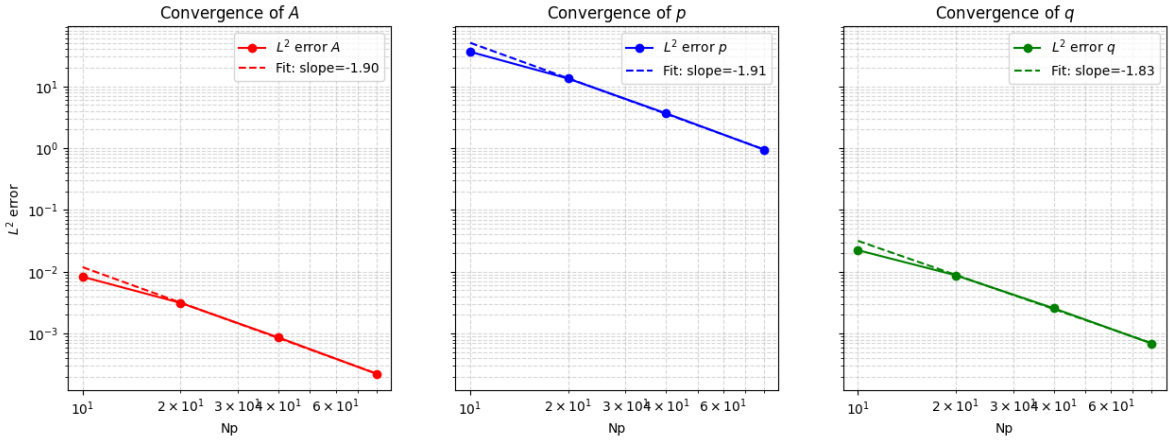

Figure 7. Convergence of numerical solution for steady validation test

Figure 7 shows the change of the L2 error for the 3 problem unknowns (q, A, p) for the steady test. In all 3 cases, the numerical convergence rate is close to the expected value of 2, corresponding to the total order of accuracy of the numerical scheme in space.

4.4 Test 4: Complete unsteady problem

Now, we consider that the cross-sectional area is changing in time:

$$\begin{aligned} A(x,t) &= t\sin(2\pi x)+4 \\ q(x,t) &= \frac{cos(2\pi x)}{2\pi} \\ p(x,t) &= p_e + K_{ref}\left(\sqrt{\frac{A(x,t)}{A_0}}-1\right)+\frac{\Gamma}{A_0\sqrt{A(x,t)}}\frac{\partial A(x,t)}{\partial t} \end{aligned} \tag{59}$$

Following a similar procedure to section 4.3, we numerically introduce the following forced source terms for the solution to be valid, yielding:

$$\hat{s}_{\text{convective}} = -\frac{t\cos^3(2\pi x)}{2\pi A(x,t)^2} - \frac{\sin(2\pi x)\cos(2\pi x)}{\pi A(x,t)} \tag{60}$$

$$\hat{s}_{\text{diffusive}} = \frac{\pi\Gamma\sqrt{A(x,t)}\cos(2\pi x)}{A_0\rho} \tag{61}$$

$$\hat{s}_{\text{pressure}} = \frac{\pi K t\sqrt{A(x,t)}\cos(2\pi x)}{\sqrt{A_0}\rho} \tag{62}$$

The results at the final time instant are presented in figure 8 and plotted against the analytical reference solution (dashed line). Again, the numerical scheme is accurately reproducing the shape of the "reference" analytical solutions.

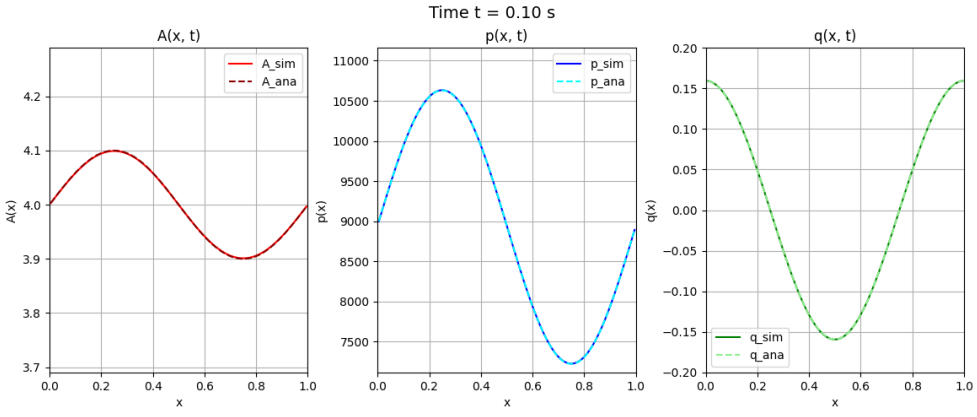

Figure 8. Cross sectional area, mass flow and pressure solution at $t = t_F$ for unsteady test ($N_p = 100$, $L = 1$ m, $A = A_0 = 3.1416\text{e-}4\ m^2$, $\Delta t = 5.10^{-3}$ s)

Figure 9 shows the change of the L2 error for the 3 problem unknowns (q, A, p) for the unsteady test. Although we should be expecting to see a spatial accuracy of second order it was only accomplished on q, the validation test for the area and pressure seems to be

performing with a spatial convergence rate closer to 1.

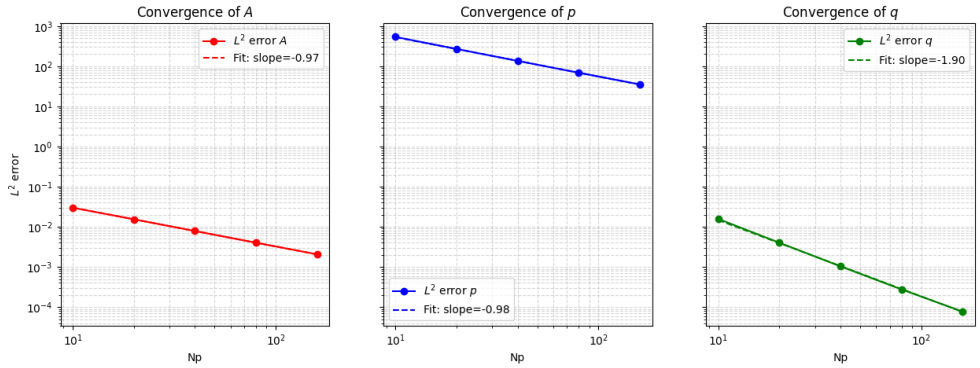

Figure 9. Convergence of numerical solution for unsteady validation test

5. Conclusions

In this work, we presented a numerical scheme to model one-dimensional flow in viscoelastic blood vessels. The underlying physical problem is based on incompressible flow governed by simplified Navier–Stokes equations, specifically the conservation of mass and momentum, along with a tube law that relates pressure to cross-sectional area. The system is solved for three unknowns: cross-sectional area, mass flow, and pressure. Our numerical methodology is based on a finite volume discretization using a staggered grid and divides the solution process into four stages: convective, diffusive, pressure, and correction. Several physical simplifications were made in the model: we assumed a one-dimensional flow (neglecting three-dimensional effects and junctions), focused only on arterial segments, neglected viscosity (hence omitting the natural velocity source term), and assumed constant stiffness with no viscoelasticity.

The scheme was validated through four different test cases, all of which produced successful results. The purely convective case showed a convergence rate slightly below the expected value of 1, with no notable differences between Ducros and Kolgan numerical schemes. The purely diffusive case showed the expected second-order convergence in space. The full steady-state problem, solved with a manufactured solution that introduced forcing terms in each stage, accurately reproduced the reference analytical profile with the expected spatial convergence rate of second order. The full unsteady case also seems to match the expected shapes of the functions, though the convergence rate seems to be off the expected order of 2.

Overall, the model demonstrated strong performance, although some open questions remain, particularly regarding the observed convergence rate for the convective schemes. The numerical scheme itself is complex, but we managed to implement it effectively by

introducing appropriate simplifications and drawing heavily from a reference paper, which despite containing some mistakes, provided valuable guidance. The use of periodic boundary conditions helped simplify the implementation, though it limited the range of physically meaningful scenarios we could test, as more realistic Dirichlet or Neumann conditions are more difficult to incorporate. The inclusion of forcing terms was essential to construct and validate the steady and unsteady test cases. While the implementation was heavy and prone to subtle errors, reliable results were ultimatealy achieved and confirmed the validity of the numerical model.

References

[1] Luca Formaggia, Alfio Quarteroni, and Alessandro Veneziani. *Cardiovascular Mathematics: Modeling and Simulation of the Circulatory System*, volume 1. Springer Science & Business Media, 2010.

[2] Alfio Quarteroni, Andrea Manzoni, and Cristian Vergara. The cardiovascular system: mathematical modelling, numerical algorithms and clinical applications. *Acta Numerica*, 26:365–590, 2017.

[3] Charles Taylor, Michael Draney, Jae Ku, David Parker, Brad Steele, Kwan-Liu Wang, and Christopher Zarins. Predictive medicine: computational techniques in therapeutic decision-making. *Computer Aided Surgery: Official Journal of the International Society for Computer Aided Surgery (ISCAS)*, 4(5):231–247, 1999.

[4] Eleuterio F. Toro. Brain venous haemodynamics, neurological diseases and mathematical modelling. a review. *Applied Mathematics and Computation*, 272:542–579, 2016.

[5] A. Lucca, Saray Busto Ulloa, Lucas Mueller, Eleuterio Toro, and M. Dumbser. A semi-implicit finite volume scheme for blood flow in elastic and viscoelastic vessels. *Journal of Computational Physics*, 495:112530, 10 2023.

[6] Eleuterio Toro and Annunziato Siviglia. Flow in collapsible tubes with discontinuous mechanical properties: Mathematical model and exact solutions. *Communications in Computational Physics*, 13, 11 2012.

[7] V. Casulli, M. Dumbser, and E. F. Toro. Semi-implicit numerical modeling of axially symmetric flows in compliant arterial systems. *International Journal for Numerical Methods in Biomedical Engineering*, 28(2):257–272, 2012.

[8] A. Malossi, P. Blanco, P. Crosetto, S. Deparis, and A. Quarteroni. Implicit coupling of one-dimensional and three-dimensional blood flow models with compliant vessels. *Multiscale Modeling & Simulation*, 11(2):474–506, 2013.

[9] M. Tavelli, M. Dumbser, and V. Casulli. High resolution methods for scalar transport problems in compliant systems of arteries. *Applied Numerical Mathematics*, 74:62–82, 2013.

[10] F. Ducros, V. Ferrand, F. Nicoud, C. Weber, D. Darracq, C. Gacherieu, and T. Poinsot. Large-eddy simulation of the shock/turbulence interaction. *Journal of Computational Physics*, 152:517–549, 1999.

[11] F. Ducros, F. Laporte, T. Soulères, V. Guinot, P. Moinat, and B. Caruelle. High-order fluxes for conservative skew-symmetric-like schemes in structured meshes: application to compressible flows. *Journal of Computational Physics*, 161:114–139, 2000.

[12] Luigi Brugnano and Vincenzo Casulli. Iterative solution of piecewise linear systems. *SIAM Journal on Scientific Computing*, 30(1):463 – 472, 2007. Cited by: 89; All Open Access, Green Open Access.

[13] Vincenzo Casulli and Paola Zanolli. Iterative solutions of mildly nonlinear systems. *Journal of Computational and Applied Mathematics*, 236(16):3937–3947, 2012. 40 years of numerical analysis: "Is the discrete world an approximation of the continuous one or is it the other way around?".

[14] Vincenzo Casulli and Paola Zanolli. A nested newton-type algorithm for finite volume methods solving richards' equation in mixed form. *SIAM Journal on Scientific Computing*, 32(4):2255–2273, 2010.